Thermo-Viscoelastic Behavior of PCNF-Filled Polypropylene Nanocomposites

Lars Frormann, Azhar Iqbal, Shahrul Azam Abdullah

Institut für Produktionstechnik, Westsächsische Hochschule Zwickau, University of Applied Sciences, Postfach 201037, Äußere Schneeberger Strasse 15-19, 08012 Zwickau, Germany

Received 30 May 2007; accepted 6 August 2007
DOI 10.1002/app.27349
Published online 15 November 2007 in Wiley InterScience (www.interscience.wiley.com).

ABSTRACT: Thermal and viscoelastic properties of composites of polypropylene (PP) filled with 0–8 vol % of vapor grown platelet carbon nanofibers (PCNF) were investigated. High shear mixing was used to disperse and distribute the nanofibers. Scanning electron microscope (SEM) was used to study the morphology of the composites that indicated the good dispersion of nanofibers within the PP matrix. Thermogravimetric analysis showed thermal stability enhancements due to the presence of PCNF in the PP matrix. DSC analysis indicated that the inclusion of nanofibers increased the melting temperature of PP matrix. By the incorporation of PCNF, the storage modulus increased whereas the mechanical loss factor (tan δ) decreased. The use and limitations of various theoretical equations to predict the storage modulus and tan δ of the fiber reinforced composites have been discussed. Cole–Cole analysis has been carried out to understand the phase behavior of the nanocomposite samples. Thermal conductivity increases from 0.125 to 0.181 W/mK. Thermal conductivity values were compared with several theoretical and semi empirical models. The van Beek model showed a very good correlation to the measured values. © 2007 Wiley Periodicals, Inc. J Appl Polym Sci 107: 2695–2703, 2008

Key words: Platelet carbon nanofibers; Polypropylene; Thermal properties; Viscoelastic properties; Thermal conductivity

INTRODUCTION

Single wall carbon nanotubes (SWNT),[1–5] multiwall carbon nanotubes (MWNT),[6–10] as well as carbon nanofibers (CNF)[11–15] are being used for reinforcing polymer matrices for improved mechanical, thermal, and electrical properties.[16] The typical diameters of SWNT are in 0.7–1.5 nm range, of MWNT in the 10–50 nm range and that for CNF in the 60–200 nm range. In SWNT and MWNT, graphitic planes are parallel to the tube axis, while in CNF, graphitic planes make a small angle to the CNF axis.[17,18]

Vapor grown carbon nanofibers (VGCNF) are noncontinuous fibers and are widely recognized today as reinforcements for polymers in many applications. The VGCNF seem promising as composite reinforcements in nanoscale technology via advantage of their high mechanical, extraordinary electrical, and thermal properties. The history of VGCNF has been described by Endo[19] and the original work of Koyama and Endo on the production and structure of VGCNF.[20] In a large number of publications[21–23] they have described their growth methods, structure, and properties related with the morphology and physical properties. The advantages of VGCNF, the technology, which is still in the developmental stage and the most promising applications for these materials are in composites; a high aspect ratio of reinforcements is required. When compared with present commercial carbons, VGCNF are much lower in cost for industrial production[24] and have excellent thermal and electrical conductivity.[25]

The prospect of low cost fabrication of VGCNF has potential to override the cost barrier that has prevented conventional carbon fiber composites from entering into cost sensitive commercial markets, particularity the electronics, aerospace, and automotive industries. Therefore, VGCNF are good reinforced filler for use in numerous commercial applications. But there are still many problems, i.e., the agglomerate of VGCNF must be overcome to give rise to best composite performance. Therefore, carbon nanofillers need to be well dispersed and aligned in polymer matrices.[6,8,26–32]

The main objective of this work has been to incorporate a new type of platelet carbon nanofibers (PCNF) with a good dispersion in polypropylene (PP) matrix. A series of such nanocomposites is prepared by melt mixing and scanning electron microscopy (SEM) was performed to investigate the morphology. Thermal properties have been investigated

Correspondence to: L. Frormann (lars.frormann@fh-zwickau.de).
Contract grant sponsor: Aif, Germany.

© 2007 Wiley Periodicals, Inc.
WILEY InterScience® DISCOVER SOMETHING GREAT

with the help of thermogravimetric analysis (TGA) and differential scanning calorimetery (DSC). The visco-elastic behavior studied with the help of dynamic mechanical analysis (DMA). Thermal conductivity was also measured as a function of temperature and filler content. Attempts have also been made to compare the experimental visco-elastic and thermal conductivity results with the values calculated by using existing theoretical models.

EXPERIMENTAL

Materials

The materials fabricated in this study were PP and PCNF. The polymer was provided by DOW Corporation Basell, Germany and its grade was H734-52RNA, with the following specifications. Density, $\rho = 0.90$ g/cm^3, MFI = 52 g/10 min, thermal conductivity, $\lambda = 0.13$ W/mK, Tensile modulus, $E = 1.6$ GPa, melting temperature, $T_M = 160$°C.

The PCNF were obtained by Future Carbon GmbH, Bayreuth, Germany with grade CNF-PL, density, $\rho = 1.95$ g/cm^3, thermal conductivity, $\lambda = 600$ W/mK, Tensile modulus, $E = 500$ GPa, diameter, $d = 100$–200 nm, length, $l = 15$–20 μm, BET-surface = 200 m^2 and percentage purity = 95%.

Composites fabrication

High shear mixing was employed to disperse the PCNF homogeneously throughout the PP matrix. Before dry blending both the polymer and PCNF, were dried in an oven at 80°C for 12 h. Mixing was performed with a Thermo Haake Rheomix 600 with mixing head operating 150 rpm at 225°C for 15 min. The speed was then raised to 180 rpm for one additional minute. The processing conditions used to fabricate the nanocomposites are optimized conditions. The optimized conditions have been attained with the help of various experiments that have been based on temperature, residence time, screw speed, and geometry. These conditions will be discussed in detail in future publication. The polymer granules were premixed with PCNF and then fed into Thermo Haake Rheomix, different volume fractions (0, 0.5, 2.5, 5.2, and 8.0%) of the PCNF filler were compounded with the polymer matrix under same conditions.

Before injection molding the PP/PCNF composites were dried again in an oven at above mentioned temperature for the same duration. The samples for the thermal conductivity and DMA analysis were prepared using a laboratory injection molding machine (All-rounder 320C 600-250, Arburg, Germany). The injection temperature was 230°C and the mold temperature was 40°C. The morphology and homogeneous distribution of PCNF within the PP matrix can be seen in Figure 1.

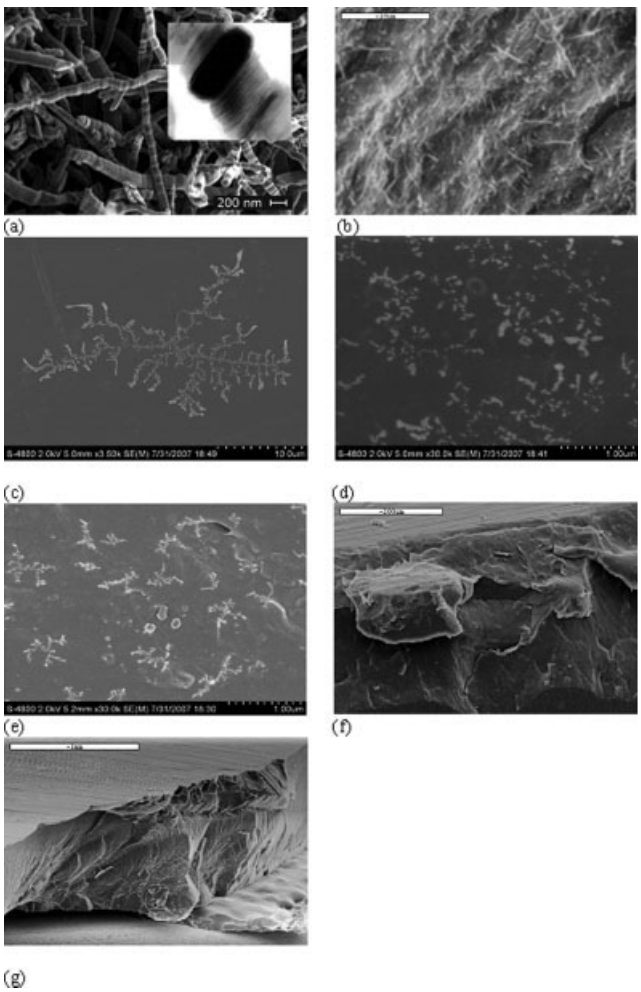

Figure 1 Scanning electron micrograph of (a) supplied PCNF (by Future Carbon), (b) PP/PCNF composite containing 0.08 volume fraction of PCNF, (c) PP/PCNF composite containing 0.052 volume fraction of PCNF, (d) PP/PCNF composite containing 0.025 volume fraction of PCNF, (e) PP/PCNF composite containing 0.005 volume fraction of PCNF, (f) freshly fractured surface of PP/PCNF containing 0.08 volume fraction of PCNF and (g) freshly fractured surface of virgin PP.

To measure the thermal conductivity disc samples of 2-mm thickness and 50-mm diameter, while for DMA the bone shaped molds with dimensions 30 × 2 × 2 mm^3 were prepared using the injection molding machine.

Experimental techniques

Scanning electron microscopy

SEM was performed to investigate the morphology of the nanocomposites with a Stereoscan-260 Cambridge Instrument. The specimens were fractured in

liquid nitrogen and coated with gold using a sputter coater, mounted and observed using EDX-detector 5431, Oxford.

Thermogravimetric analysis

TGA of unfilled PP and PCNF filled composites was analyzed by TGA-2950 (TA Instruments, Alzenau, Germany). All the specimens weighing 3–8 mg were heated from 0 to 700°C with 20°C/min under a nitrogen purge. The instrument temperature calibration was performed by using the curie temperature of various metals according to the manufacturer's recommendations.

Differential scanning calorimetry

DSC measurements were investigated by conventional differential scanning calorimeter DSC-2920 (TA Instruments, Alzenau, Germany). Samples with a weight of ~ 8–10 mg were placed in aluminium pans and a constant nitrogen flow of 35 mL/min was used to purge the instrument. Measurements were performed from 0 to 300°C with heating rate of 10°C/min. The instrument was calibrated in the same temperature range using sapphire (Al_2O_3) sample with a well known specific heat capacity as standard. The accuracy of the measurements is 3%.

Dynamic mechanical analysis measurements

The DMA was done by DMA-2980 (TA Instruments, Alzenau, Germany) in forced vibration single cantilever mode with a frequency of 10 Hz and the amplitude of 20 μm. The temperature scan ranged from −40 to 180°C with 2°C/min. A constant nitrogen flow of 40 mL/min was used to purge the instrument. Small bone ($30 \times 2 \times 2$ mm^3) shaped specimens were used for the measurement of storage modulus, loss modulus and damping factor as a function of temperature. The instrument was calibrated for temperature by using a standard mass and probe position. Furnace and eigenvalue calibrations were also performed. Three samples have been tested for each scan and the error was less than 2%.

Thermal conductivity measurements

Thermal conductivity was measured using TCA Thermal Conductivity Analyzer (TCA-200LT-A, Netzsch, Selb, Germany) with the guarded heat flow meter method. The injection molded samples (discs with 2-mm thickness and 50-mm diameter) were placed between two heated surfaces controlled at different temperatures with a flow of heat from the hot to the cold surface. When thermal equilibrium was attained thermal conductivity data were taken within an accuracy of 4%.

Theoretical considerations

Theoretical prediction of storage modulus

One of the simplest equations for the reinforcement of a material due to an inclusion was given by Einstein.[33]

$$G_c = G_m(1 + 1.25\,V_f) \tag{1}$$

where G is the storage modulus, subscripts c and m stands for composite and matrix, respectively, V_f is the volume fraction of the PCNF inclusions. Another equation proposed by Einstein was

$$G_c = G_m(1 + V_f) \tag{2}$$

where the terms are the same as explained above. The modification of Einstein's equations was done by Guth[34] and his proposed equation was

$$G_c = G_m(1 + 2.5V_f + 14.1V_f^2) \tag{3}$$

Another modification was made by Cohan that resulted in the equation.[35]

$$G_c = G_m(1 + 0.675\rho + 1.62\rho^2 V_f + 14.1V_f^2) \tag{4}$$

where ρ is the aspect ratio of the fibers and the modification suggested by Mooney[36] was

$$G_c = G_m \exp\left(\frac{2.5V_f}{1 - SV_f}\right) \tag{5}$$

where S is crowding factor or relative sedimentation volume of the inclusion and is mathematically defined as the ratio of apparent volume occupied by the fiber to the true volume of the fiber.

Theoretical prediction of tan δ values

Rigid fillers usually decrease the damping as expressed by mechanical loss factor (tan δ) to an extent predicted by a rule of mixture equation.[37]

$$\tan\delta_c = V_f \tan\delta_f + V_m \tan\delta_m \tag{6}$$

In case of rigid inclusions the first term can be neglected and the equation becomes[38]

$$\tan\delta_c = V_m \tan\delta_m \tag{7}$$

where the subscripts c and m represent composite and matrix, V_m is the volume fraction of the matrix.

TABLE I
Selected Models of Thermal Conductivity

Name of models	Equations	Equation no.
Bruggeman	$\lambda_e = \frac{\lambda_m}{(1-f)^3}$	(9)
Böttcher	$\lambda_e = \frac{\lambda_m}{(1-f)}$	(10)
de Loor ($f < 0.2$)	$\lambda_e = \lambda_m \frac{1+f}{1-2f}$	(11)
van Beek ($f < 0.2$)	$\lambda_e = \lambda_m \frac{1-f}{1-4f}$	(12)
Agari-Uno	$\lambda_e = \exp[fC_2 \log(\lambda_c) + (1-f) \log(C_1\lambda_m)]$	(13)
Ce-Wen Nan	$\lambda_e = \lambda_m \frac{3+f\lambda_c/\lambda_m}{3-2f}$	(14)
Ce-Wen Nan ($f < 0.1$) with interface effect	$\lambda_e = \lambda_m \left[1 + \frac{fp}{3} \frac{\lambda_c/\lambda_m}{p+\frac{2a_k}{d}\frac{\lambda_c}{\lambda_m}}\right]$	(15)

The eq. (7) must have some stiffness parameter because it is assumed that the matrix in the presence of fibers offers a stiffness equivalent to the minimum elastic modulus of the composite; then above equation was modified as[39]

$$\tan \delta_c = V_m(G_m/G_c) \tan \delta_m \quad (8)$$

where V_m, tan δ, c and m are as explained above, G is the storage modulus of the material. For details of the models the reader is referred to the cited works.

Selected theoretical models for thermal conductivity

A number of classical models by Bruggeman,[40] Böttcher,[41] deLoor,[42] van Beek,[43] Agari and Uno,[44] Nan et al.,[45] a simple model for thermal conductivity of carbon nanotubes (CNT) based composites and Nan et al.[46] model taking into account the interface effect on thermal conductivity of CNT composites have been applied to calculate the thermal conductivity in two component systems of PP and PCNF composites. For the sake of simplification it is assumed that no interaction is present amongst the fillers and the filler property λ_c is much larger than the property λ_m of the matrix material.[47] Here λ_e, λ_m, and λ_c denote the effective thermal conductivity of the composite, matrix and filler, respectively, and f denotes the volume fraction of the PCNF. All the selected models are presented in Table I.

In eq. (13) C_1 describes the influences on crystallinity and C_2 describes the ease of forming conductive networks of fillers within the polymer matrix. While in eq. (15), here p, d denotes the aspect ratio and diameter of PCNF, respectively, and $a_k = R_k\lambda_m$, where the interface thermal resistance is known as the Kapitza resistance, R_k. The interface thermal resistance across the CNT and matrix reported by Huxtable et al.[48] is about 8.3×10^{-8} m^2 K/W. So in case of PP, a_k = 10.79 nm. The other terms are the same as stated above.

RESULTS AND DISCUSSION

Morphological characterization

The morphology of PP/PCNF composites was evaluated by SEM to observe the distribution of nanofibers within the injection molded disc samples. All specimens are mounted such that the plane viewed under the microscope is a cross-sectional cut parallel and perpendicular to the flow direction of injection molding. Figure 1(a) show the SEM micrograph of PCNF provided, showing potentially reactive carbon edge-sites on the entire nanofiber surface that could be responsible to enhance the strength and thermal conductivity of composite materials. While Figure 1(b–e) give the micrograph of composites with 8.0–0.5 vol % of PCNF parallel to the flow direction of injection molded specimens indicating that the nanofibers are well dispersed in the PP matrix. Figure 1(f) gives the fracture surface of the 8 vol % of composite perpendicular to the flow direction. Good nanofiber dispersion is also clearly seen in the PP/PCNF composite. Figure 1(g) shows the micrograph of unfilled PP. The close observation of Figure 1(f) gives a clue about a thin layer of polymer on the flat surface of injection molded samples that could create a negative impact in measuring the thermal conductivity perpendicular to the flat surface of injection molded discs.

Thermogravimetric analysis

Figure 2 presents the analysis of degradation of the injection molded PP/PCNF composites and unfilled PP under nitrogen. The figure shows excellent agreement amongst the curves containing various amounts of PCNF. From the figure it can be seen

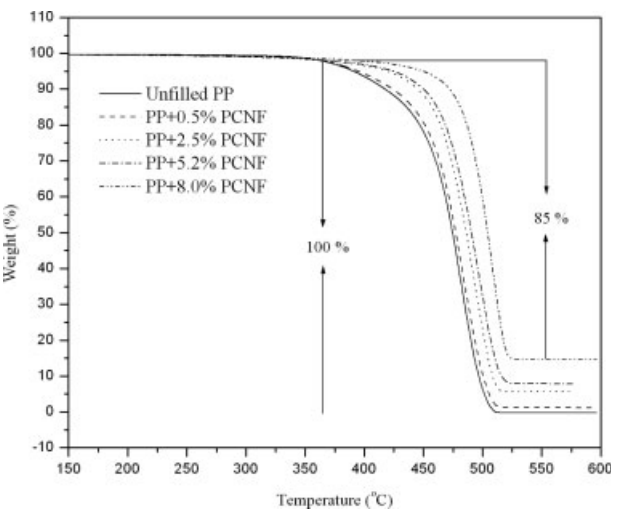

Figure 2 TGA thermogram of pure PP and PP/PCNF nanocomposites containing various amounts of PCNF by vol %.

that the virgin PP has the highest weight loss as a function of temperature followed by an excellent agreement of composites consisting of various volume fractions of PCNF. Nearly 15% weight loss has been reduced in the composites containing the filler fraction up to 0.08 by volume. The nanofiber reinforced composites showed higher thermal stability than pure PP. The degradation onset temperature is higher and the residue amount is also higher at the same temperature, it is because of the high thermal stability of nanofiber itself and the restriction effect of nanofibers on the polymer chains. The results are in consistent to previously published results for other matrices.[32,49]

Differential scanning calorimetry analysis

The differential scanning calorimetry (DSC) results are shown by Figure 3 of pure PP and PP/PCNF composites. The DSC measures the difference in heat flow to or from a specimen due to thermal reactions as a function of temperature. The endotherm between 150 and 180°C represents the melting of spherulites in the matrix. The figure also suggested that the addition of PCNF to the PP caused only a marginal effect on T_m (melting temperature) and no correlation of the results with the filler concentration can be established. Crystallization temperature and enthalpy of crystallization of the PP phase increased with increasing content of CNF, indicating that fillers nucleate the crystallization process. It seems from the melting peak that the presence of PCNF has decreased the crystallinity of the PP matrix. As the concentration of PCNF increased, the nanofibers acted to restrict the sites of PP segments, obstructing them from obtaining a highly ordered spherulite structure and the crystallinity decreased.[15]

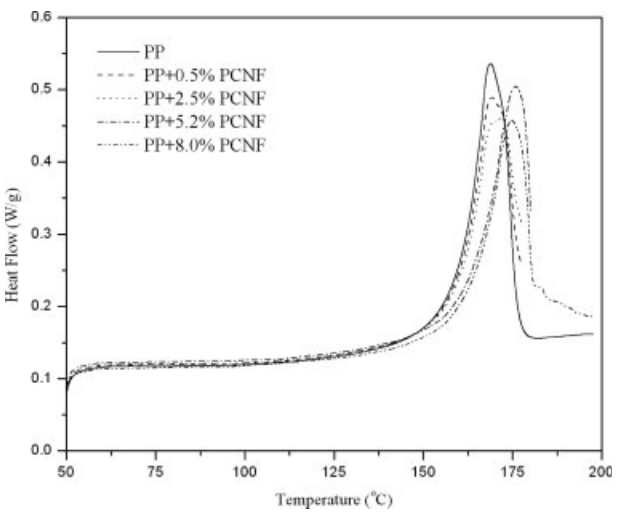

Figure 3 DSC thermogram of virgin PP and PP/PCNF composites consisting of various amounts of PCNF by vol %.

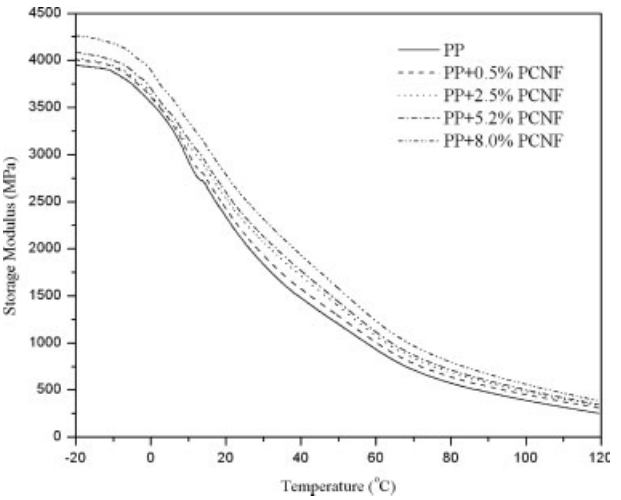

Figure 4 Storage modulus vs. temperature for pure PP and PP/PCNF nanocomposites consisting of various amounts of PCNF by vol %.

Dynamic mechanical analysis

The storage modulus against temperature of injection molded PP/PCNF composites and pure PP is presented in Figure 4. The results show the effect of fibers concentration on the stiffness of nanocomposites. In addition, the presence of CNF also enables the matrix to sustain a high modulus value at high temperatures. At 20°C the addition of 0.5 and 8.0 vol % results in a 5 and 20% increase in storage modulus for nanocomposites, respectively. With the increase of temperature to melting temperature the modulus decreases sharply and tends to approach to that of pure PP, indicating that at high temperature, the modulus of the composites were dominated by the matrix intrinsic modulus. This phenomenon was also observed by other researchers when working with polyethylene, ABS and polystyrene composites.[15,32,50]

Figure 5 represents the damping factor vs. temperature curves for unfilled PP and PP/PCNF composites containing various volume fractions of PCNF. The damping factor (tan δ) increase first, reaches a maximum at the glass transition temperature (β-transition), decrease and again reaches a maximum due to α-transition. β-relaxation peak is located between 10 and 25°C. Peak height shows the temperature at which maximum heat dissipation occurs. The pure PP and all the PP/PCNF composites exhibit a damping peak. From Figure 5, it is also obvious that the inclusion of CNF lowers the peak position of tan δ. This reflects the interaction effects of CNF to the relaxation of the polymer chains.[51,52]

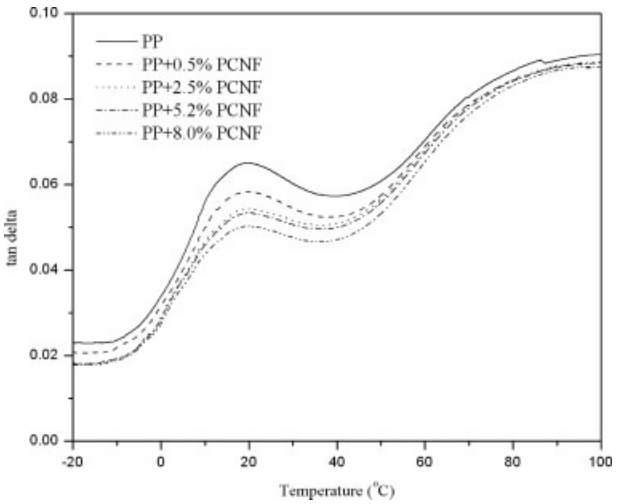

Figure 5 Mechanical loss factor vs. temperature behavior of unfilled PP and PP/PCNF nanocomposites consisting of various amounts of PCNF by vol %.

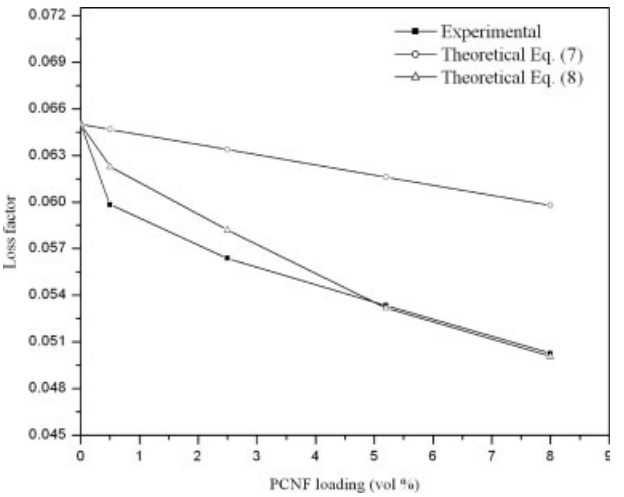

Figure 7 Plots of experimental and theoretical loss factor values against PCNF loading at 20°C.

Cole–Cole plots of unfilled PP and PP/PCNF are depicted in Figure 6. Generally, homogeneous polymeric systems exhibit a semicircle while two-phase systems show two modified circles.[53,54] It can be seen from the figure that the pure PP tends to form a half circle but as the amount of the PCNF increase departure from the semi-circle occurs. So this suggested that the nanocomposites show a different behavior from homogeneous system, may be it is attributed to the existence of different interphase effects and microscopically heterogeneous dispersion of nanofibers within the PP matrix.[37]

The plots of experimental and theoretical loss factor (tan δ) values of PP/PCNF against loadings of PCNF as various volume fractions are presented in Figure 7. So it has been confirmed again that very small amount of PCNF impart stability to PP matrix, because the experimental curve lies below to both of the theoretical curves. It can also be seen from the figure that, the eq. (8) agrees better than eq. (7) with the experimental values. The deviations shown by the models from the experimental data may be due to the reason that both the equations ignore the localized constraints imposed by the nanofibers on PP matrix deformation. Moreover, the transcrystallinity of PP has not been considered by these equations. The results are in accordance with the other authors.[37]

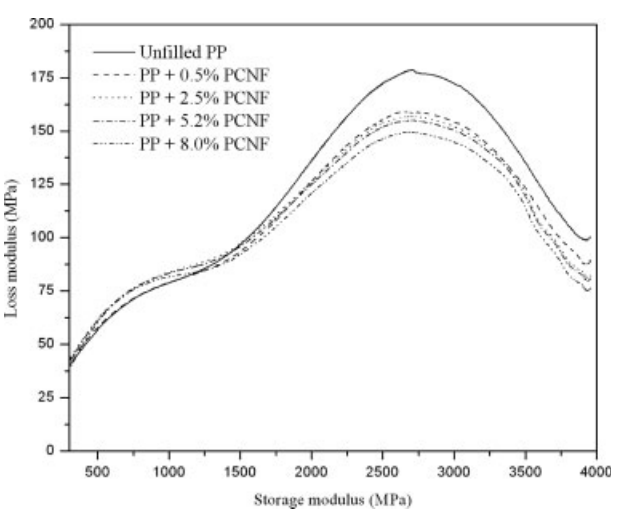

Figure 6 Cole-Cole plots of unfilled PP and PP/PCNF nanocomposites containing various amounts of PCNF by vol %.

The experimental and theoretical storage moduli values at 20°C for various loadings of PCNF by vol % are given in Table I. It can be observed from the table that at 0.5 vol % of nanofibers loading, in all the models, Einstein's [eqs. (1) and (2)], Guth [eq. (3)] and Mooney [eq. (5), $S = 1$ and $S = 1.35$) show slight negative deviation from the experimental values. Except Cohan model [eq. (4)], the aspect ratio term ρ gives the extra higher values (in case of PCNF $\rho = 130$), therefore higher values are obtained in all the cases. This gives a clear indication that even a very small loading of PCNF increase the storage moduli of PP matrix than expected. It can also be attributed to the fact that PCNF have potentially reactive carbon edge-sites on the entire nanofiber surface [as shown in Fig. 1(a)] and therefore, better interaction of PCNF-PP is responsible to increase the storage modulus even at lower loadings.[55] The same trend can be observed with 2.5 vol % of nanofibers but at 5.2 vol %, Guth model gives slightly higher value. The agreement shown by Mooney model is because of the presence of crowding factor in the equation. At 8 vol % nanofiber loading, Einstein's models deviate from the experimental values by 7.8–9.5%, where as at same nanofiber loading Guth and

Mooney models give the higher storage moduli values than the experimental. The general nature of Mooney equation, i.e., a modulus value tends to infinity at higher loadings that is previously reported,[56] can be observed here too. Mooney equation agrees better with $S = 1.35$ at lower loadings and $S = 1$ at higher loadings of PCNF. Einstein's equations present lower values at all the volume fractions of PCNF.

Thermal conductivity studies

The thermal conductivity of the unfilled PP and PP/PCNF composites as a function of temperature are shown in Figure 8. As one can observe, the thermal conductivities in composites increase with the volume fraction of PCNF. In the PP/PCNF composites with 0.005 volumes fraction of PCNF increases the thermal conductivity $\sim$ 18% higher than that of pure PP while, at 0.08 volume fraction this increase is almost 45%. This fact can be attributed to intrinsic thermal conductivity of the PCNF and their large aspect ratio ($\sim$ 130) that even at lower loadings of nanofibers are effective to form heat conduction bridges to transfer heat through the sample. At a higher volume fraction, this effect becomes stronger. The thermal conductivity values of the virgin PP and PP filled with various fractions of PCNF are increased only slightly as a function of temperature.

Figure 9 presents the theoretically predicted thermal conductivity values of several theoretical models and experimentally estimated thermal conductivity of PP/PCNF composites. It can be observed that the models Bruggeman,[40] deLoor,[42] and van Beek[43] give pretty fine correlation to the measured values in the investigated filler fraction loading and temperature region. Böttcher[41] model gives much lower values,

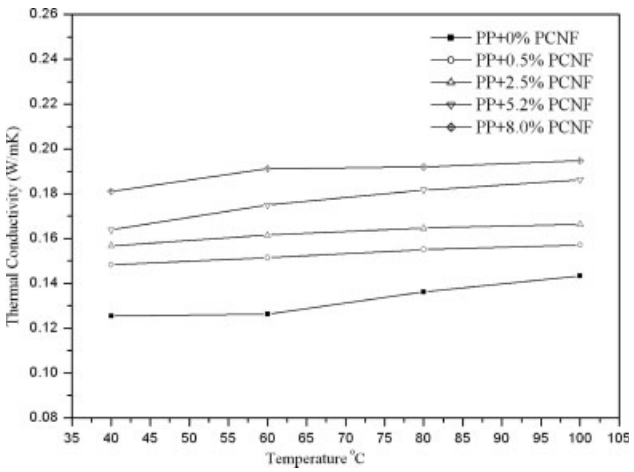

Figure 8 Thermal conductivity of PP/PCNF composites as a function of temperature consisting of various amounts of PCNF by vol %.

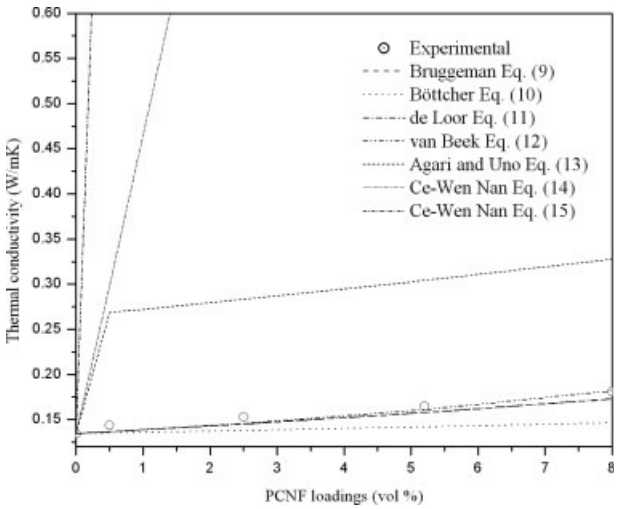

Figure 9 Comparison of measured thermal conductivity values of unfilled PP and PP with various amounts of PCNF by vol % with several theoretical models described in eqs. (9)–(15) at 40°C. The lines are describing the theoretical values, while symbols represent measured values.

but the van Beek model gives the best agreement to the experimental values especially at higher volume fractions of nanofibers. However, Agari and Uno[44] model consists of two fit parameters C_1 and C_2, which are unknown and can be found by the best linear fit to the measurement data. As expected, Nan et al. models[45,46] give extremely high values when compared with the experimental values. These discrepancies can be explained by the fact that these two models have been designed for CNT composites and these CNT has thermal conductivity almost in the range of 3000 W/mK when compared with PCNF whose thermal conductivity is almost 600 W/mK. Since, in these models the effective thermal conductivity of composites is directly related to the thermal conductivity of fillers.

Anomalies between theoretical and measured values occurs due to the fact that thermally conductive PCNF in a polymer matrix do not form a perfect conductive network but a network with a worse quality of thermal contacts that can be described by the interconnectivity of the particles.[47,57] The interconnectivity of PCNF with the polymer matrix lies between the perfect network, in case of CNT having very long aspect ratio ($\sim$ 1000) and the particles ($\sim$ 1), as the results are clearly manifested by Figure 9.

CONCLUSIONS

The PP/PCNF composites revealed the successful exploitation of PCNF as reinforcements for PP matrix in conventional processing techniques such as extrusion and injection molding. Scanning electron microscope (SEM) indicated the good dispersion of

TABLE II
Comparison of Experimental and Theoretical Storage Moduli Values of Unfilled PP and PP/PCNF Composites at 20°C for Different Loadings of PCNF

PCNF loading (vol %)	Storage modulus (GPa)						
	Experimental values	Einstein[33] eq. (1)	Einstein[33] eq. (2)	Guth[34] eq. (3)	Cohan[35] eq. (4)	Mooney[36] eq. (5) $S = 1$	Mooney[36] eq. (5) $S = 1.35$
0	2.323	2.323	2.323	2.323	2.323	2.323	2.323
0.5	2.412	2.338	2.335	2.353	543.7	2.352	2.353
2.5	2.529	2.396	2.381	2.489	1875.1	2.477	2.478
5.2	2.691	2.474	2.444	2.714	3672.5	2.664	2.672
8.0	2.773	2.555	2.509	2.997	5536.5	2.887	2.907

nanofibers within the PP matrix. SEM micrograph of PCNF provided, showed potentially reactive carbon edge-sites on the entire nanofiber surface that may enhanced the strength and thermal conductivity of the composites even at lower nanofiber loadings owing to enhanced filler-matrix interaction.

TGA showed thermal stability enhancements due to the presence of PCNF in the PP matrix. This stability enhancement was raised up to 15% at 550°C with a nanofiber loading of 0.08 volume fraction. DSC analysis indicated that the inclusion of nanofibers increased the melting temperature and decreased the crystallinity of PP matrix acting as restriction sites for the PP segments and obstructing them from obtaining a highly ordered spherulite structure.

In DMA, the storage modulus (G) drops upon increasing the temperature due to increased segmental mobility, but the presence of CNF enabled the matrix to sustain a high G value even at high temperatures. Reduction in storage modulus with increase in temperature is associated with softening of the matrix at higher temperatures. The damping factor (tan δ) increases first, reaches a maximum at the glass transition temperature (β-transition), decreases and again reaches a maximum due to α-transition. As the volume fraction of nanofibers increased, the value of damping factor decreased due to the improved PCNF-PP interfacial adhesion. The Cole–Cole plot of the composites indicated the heterogeneous nature of the system. Applicability of various models to predict the storage modulus and damping factor of the composites was checked and it was found that the experimental values lie close tothe most of the models.

The thermal conductivity was increased from λ = 0.125–0.181 W/mK for PP filled with 8 vol % of PCNF. Measurement values can be described by Bruggeman, de Loor and van Beek models in an appropriate way in the investigated range of filler fraction. Böttcher model gave lower, Agari and Uno model gave much higher values and Ce-Wen Nan gave extremely high values. This was due to the factor that interconnectivity of PCNF lies between CNT and particles within the polymer host.

Authors thank Prof. Dr. Wieland Zahn and Ms. Karla Pawlik for their help in providing the SEM micrographs of composites. The authors also thank Florian Michl (Future Carbon GmbH, Bayreuth, Germany) for supplying platelet carbon nanofibers.

References

1. Yakobson, B. I.; Smalley, R. E. Am Sci 1997, 85, 324.
2. Shaffer, M. S. P.; Windle, A. H. Adv Mater 1999, 11, 937.
3. Shpak, A. P.; Kolesnik, S. P.; Mogilny, G. S.; Petrov, Y. N.; Sokhatsky, V. P.; Trophimova, L. N.; Shnina, B. D.; Gavriljuk, V. G. Acta Mater 2007, 55, 1769.
4. Park, C.; Ounaies, Z.; Watson, K. A.; Crooks, R. E.; Smith, J.; Lowther, S. E.; Connell, J. W.; Siochi, E. J.; Harrison, J. S.; Clair, S. T. L. Chem Phys Lett 2002, 364, 303.
5. Lillehei, P. T.; Park, C.; Rouse, J. H.; Siochi, E. J. Nano Lett 2002, 2, 827.
6. Qian, D.; Dickey, E. C.; Andrews, R.; Rantell, T. Appl Phys Lett 2000, 76, 2868.
7. Jin, L.; Bower, C.; Zhou, O. Appl Phys Lett 1998, 73, 1197.
8. Schadler, L. S.; Giannaris, S. C.; Ajayan, P. M. Appl Phys Lett 1998, 73, 3842.
9. Lau, K. T.; Shi, S. Q. Carbon 2002, 40, 2965.
10. Cumings, J.; Zettl, A. Science 2000, 289, 602.
11. Kumar, S.; Doshi, H.; Srinivasarao, M.; Park, J. O.; Schiraldi, D. A. Polymer 2002, 43, 1701.
12. Dasch, C. J.; Baxter, W. J.; Tibbetts, G. G. In 21st Bienn Conference on Carbon, Buffalo, NY, 1993; p 82.
13. Carneiro, O. S.; Covas, J. A.; Bernardo, C. A.; Caldiera, G; Van Hattum, F. W. J.; Ting, J. M.; Alig, R. L.; Lake, M. L. Compos Sci Technol 1998, 58, 401.
14. Lozano, K.; Bonilla-Rios, J.; Barrera, E. V. J Appl Polym Sci 2001, 80, 1162.
15. Lozano, K.; Barrera, E. V. J Appl Polym Sci 2000, 79, 125.
16. Lau, K. T.; Hui, D. Compos B 2002, 33, 263.
17. Ma, H.; Zeng, J.; Realff, M. L.; Kumar, S.; Schiraldi, D. A. Compos Sci Technol 2003, 63, 1617.
18. Zeng, J.; Saltysiak, B.; Johnson, W. S.; Schiraldi, D. A.; Kumar, S. Compos B 2004, 35, 245.
19. Endo, M. Chem Technol 1988, 18, 568.
20. Koyama, T. Carbon 1972, 10, 757.
21. Tibbetts, G. G.; Doll, G. L.; Gorkiewicz, D. W.; Moleski, J. J.; Perry, T. A.; Dasch, C. J. Carbon 1993, 31, 1039.
22. Heremans, J.; Rahim, I.; Dresselhaus, M. S. Phys Rev B 1985, 32, 6742.
23. Van Hattum, F. W. J.; Serp, P.; Figueiredo, J. L.; Bernardo, C. A. Carbon 1997, 35, 860.
24. Beck, S. In Proceedings of the Fourth Annual Conference on Advanced Composites. ASM International Congress: Dearborn, MI, 1988; p 463.

25. Young, K. C.; Koh, I. S.; Sung, M. S.; Morinobu, E. Compos A 2006, 37, 1944.
26. Allaoui, A.; Bai, S.; Cheng, H. M.; Bai, J. B. Compos Sci Technol 2002, 62, 1993.
27. Satish, K.; Doshi, H.; Srinivasarao, M.; Park, J. O.; Schiraldi, D. A. Polymer 2002, 43, 1701.
28. Patton, R. D.; Pittman, C. U.; Wang, L.; Hill, J. R. Compos A 1999, 30, 1081.
29. Sandler, J.; Werner, P.; Shaffer, M. S. P.; Demchuk, V.; Altstadt, V.; Windle, A. H. Compos A 2002, 33, 1033.
30. Bower, C.; Rosen, R.; Jin, L.; Han, J.; Zhou, O. Appl Phys Lett 1999, 74, 3317.
31. Choi, Y. K.; Sugimoto, K. I.; Song, S. M.; Endo, M. Mater Lett 2005, 59, 3514.
32. Yang, S.; Taha, T. J.; Serrato, D. V.; Hernandez, K.; Lozano, K. Compos B 2007, 38, 228.
33. Einstein, A. Investigation on Theory of Brownian Motion; Dover: New York, 1956.
34. Guth, E. J Appl Phys 1945, 16, 20.
35. Joseph, P. V.; Mathew, G.; Joseph, K.; Groeninckx, G.; Thomas, S. Compos A 2003, 34, 275.
36. Mooney, M. Colloid Sci 1951, 6, 162.
37. Nielsen, L. E. Mechanical Properties of Polymers and Composites; Marcel Dekker: New York, 1974; Vol. 2, Chapter 7.
38. Drzal, L. T.; Rich, M. J.; Koenig, M. F.; Llyod, P. F. Adhesion 1983, 16, 133.
39. Tung, C. M.; Dynes, P. J. J Appl Polym Sci 1987, 33, 505.
40. Bruggeman, D. Ann Phys 1935, 24, 636.
41. Böttcher, C. Theory of Electric Polarisation; Elsevier: Amsterdam, The Netherlands, 1952.
42. deLoor, G. PhD Thesis, University of Leiden, NL: Leiden, 1956.
43. van Beek, L. Prog Dielect 1967, 7, 69.
44. Agari, Y.; Uno, A. J Appl Polym Sci 1986, 32, 5705.
45. Nan, C. W.; Shi, Z.; Lin, Y. Chem Phys Lett 2003, 375, 666.
46. Nan, C. W.; Liu, G.; Lin, Y.; Li, M. Appl Phys Lett 2004, 85, 3549.
47. Razzaq, M. Y.; Anhalt, M.; Frormann, L.; Weidenfeller, B. Mater Sci Eng A 2007, 444, 227.
48. Huxtable, S.; Cahill, D. G.; Shenogin, S.; Xue, L.; Ozisik, R.; Barone, P.; Usrey, M.; Strano, M. S.; Siddons, G.; Shim, M.; Keblinski, P. Nat Mater 2003, 2, 731.
49. Zhu, J.; Peng, H.; Rodriguez-Macias, F.; Margrave, J. L.; Khabashesku, V. N.; Imam, A. M.; Lozano, K.; Barrera, E. V. Adv Funct Mater 2004, 14, 643.
50. Jin, Z.; Pramoda, K. P.; Xu, G.; Goh, S. H. Chem Phys Lett 2001, 337, 43.
51. Saleem, A.; Iqbal, A.; Frormann, L. Polym Res 2007, 14, 121.
52. Iqbal, A; Frormann, L; Saleem, A; Ishaq, M. Polym Compos 2007, 28, 186.
53. Aklonis, J. J.; Macknight, W. J. Introduction to Viscoelasticity; Wiley: New York, 1983.
54. Ibarra, L.; Macías, A.; Palma, E. J Appl Polym Sci 1995, 57, 831.
55. Zhong, W. H.; Li, J.; Lukehart, C. M.; Xu, L. R. Polym Compos 2005, 26, 128.
56. Nielsen, L. E. Compos Mater 1967, 1, 100.
57. Weidenfeller, B.; Höfer, M.; Schilling, F. Compos A 2004, 35, 423.